IEEE Access
Multidisciplinary ⋮ Rapid Review ⋮ Open Access Journal

Received 2 February 2023, accepted 16 February 2023, date of publication 22 February 2023, date of current version 27 February 2023.

Digital Object Identifier 10.1109/ACCESS.2023.3247137

RESEARCH ARTICLE

Design of Compact Quasi-Elliptic Bandpass Filters Based on Coaxial Inset Resonators

ABDULRAHMAN WIDAA, (Graduate Student Member, IEEE), CHAD BARTLETT, (Graduate Student Member, IEEE), AND MICHAEL HÖFT, (Senior Member, IEEE)

Chair of Microwave Engineering, Kiel University, 24143 Kiel, Germany

Corresponding author: Abdulrahman Widaa (aw@tf.uni-kiel.de)

This work was supported in part by the European Union's Horizon 2020 Research and Innovation Program under the Marie Skłodowska-Curie under Agreement 811232-H2020-MSCA-ITN-2018, and in part by the DFG Open Access Publication Funding Program of Kiel University.

ABSTRACT This article reports a novel *inset resonator* configuration for coaxial filter applications with quasi-elliptic responses. The design and analysis of the inset resonator are discussed in detail and accurately modeled as a capacitively-loaded stepped-impedance half-wavelength resonator featuring more compactness, high quality factor, and enhanced spurious responses in comparison with conventional half-wavelength and combline resonators. Additionally, the operating frequency can be tuned intrinsically through the displacement of the coaxial resonator, eliminating the need for any additional tuning elements and maintaining a stable quality factor. Two quasi-elliptic inset resonator type filters are implemented in planar and longitudinal coupling configurations, respectively. The first takes the form of a folded four-pole 2.93 GHz filter with two symmetrical transmission zeros. The fabricated filter has a compact structure of 29.76 cm^3, an insertion loss better than 0.73 dB, a return loss better than 18 dB, and a wide spurious-free band up to $3.5{\cdot}f_0$. The second inset-type quasi-elliptic filter is realized in a longitudinal inline arrangement. An example of a 2.53 GHz three-pole filter is presented with a closely-positioned transmission zero, wide spurious-free band ($\approx 3{\cdot}f_0$), and a very compact structure of $55.7\times33\times33$ mm^3.

INDEX TERMS Coaxial filter, inset resonator, miniaturization, passive components, tunable filters, waveguide technology.

I. INTRODUCTION

Compact coaxial microwave filters with high-Q and excellent spurious rejection performance are essential components for a broad range of evolving applications including cellular base stations and satellite payloads. In common, coaxial filters are realized using half-wavelength and combline resonators. However, from one side, the large bulky structures and poor spurious performance of the $\lambda/2$ resonators make them an unfavorable option, except in very specific applications such as [1] and [2]. In [1], freely movable resonators were required to design a frequency-tunable coaxial filter. Whereas in [2], $\lambda/2$ dielectric resonators were employed to satisfy a high-Q requirement for satellite multiplexer applications. According to the authors knowledge, these two coaxial filters are the only available examples in the literature based on $\lambda/2$ resonators. It is worth noting that both designs have bulky structures and poor spurious performance, as expected. On the other hand, combline resonators widely dominate coaxial filters research due to their compact structures with mid-high Q and wide spurious-free bands ($>3{\cdot}f_0$). Similarly, as more compactness and volume-saving are always required, various miniaturized combline filters were presented with good spurious performance based on different configurations [3], [4], [5], [6], [7], [8], [9], [10], [11], [12], [13], [14]. Several of these designs have employed stepped-impedance resonators (SIRs) where the top end of the combline post is enlarged to increase capacitive loading, providing more miniaturization and increasing the band separation to the next spurious

The associate editor coordinating the review of this manuscript and approving it for publication was Giorgio Montisci.

resonance [3], [4], [5], [6], [7], [8]. However, this class of filter must take into account weak inter-resonator couplings, manufacturing complexity, and the added weight of the enlarged parts. The second group of miniaturized combline filters employs multiple interlaced compact re-entrant resonators as demonstrated in [9], [10], and [11]. These filters also have relatively complex structures, limited high-power handling capabilities, and increased losses. Recently, 3D printing was used to fabricate non-conventional geometries of compact combline filters in vertical alignments [12], [13], [14]. Looking at all of these aforementioned combline-based designs, we can see that there is a appreciable space for the exploration of alternative designs to enable easier manufacturing, and more flexible resonators types.

Besides miniturization and good spurious responses, coaxial filters often require transmission zeros (TZs) at one or both stopbands to meet rejection specifications. Commonly, coupling probes and folded configurations are needed to realize the cross-coupling required for TZs' creation, such as the designs in [15] and [16]. However, these probes can resonate and create unwanted spurious resonance close to the passband. Moreover, many applications require inline configurations where the input and the output are on opposite sides. Therefore, [17] and [18] presented inline cross-coupled combline filters using an orthogonal resonator arrangement without the need for any coupling probes. Here, it can be noted that the manufacturing of such orthogonal combline structures is complex and costly. Another method of introducing TZs in inline combline filters uses strongly coupled doublets and triplets as demonstrated in [19] and [20]. Unfortunately, this mechanism has many design challenges including unwanted spurious resonances, decreased Q-factor, and limited flexibility of the TZs. Considering the above-mentioned drawbacks, we can conclude that the introduction of inline coaxial filters with easy creation and flexible control of TZs is greatly appreciated.

In [21], we introduced the novel *inset*-type coaxial resonator configuration for both fixed and tunable microwave filters and components with simple, proof-of-concept single-cavity and two-pole filter examples. The proposed inset resonator configuration provides many desirable advantages including the compact structure, good spurious performance, comparably high Q-factor, and efficient *self-tuning*. Hereafter, [21] is extended into two research articles: the presented work here which discusses the design process of the coaxial inset resonators and their application to fixed quasi-elliptic bandpass filters, and [22] which details the design of high-Q tunable filters with constant absolute bandwidth based on inset resonators. The main contributions of this paper are summarized as follows:

- Detailed modeling and analysis procedure of the inset-type resonator is provided, and different design parameters are investigated.
- A 4-pole quasi-elliptic filter is implemented in a folded planar coupling configuration, and the measured results are reported.

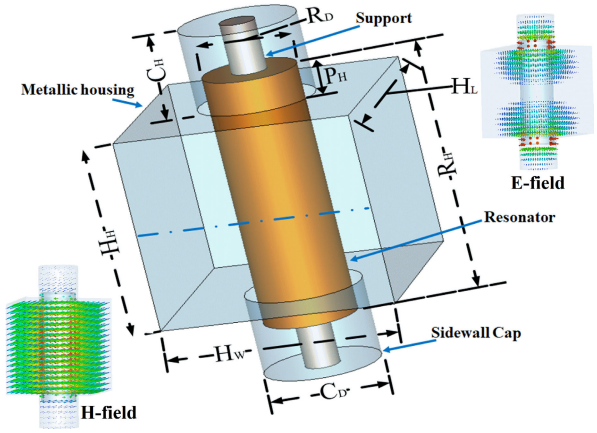

FIGURE 1. Inset resonator structure.

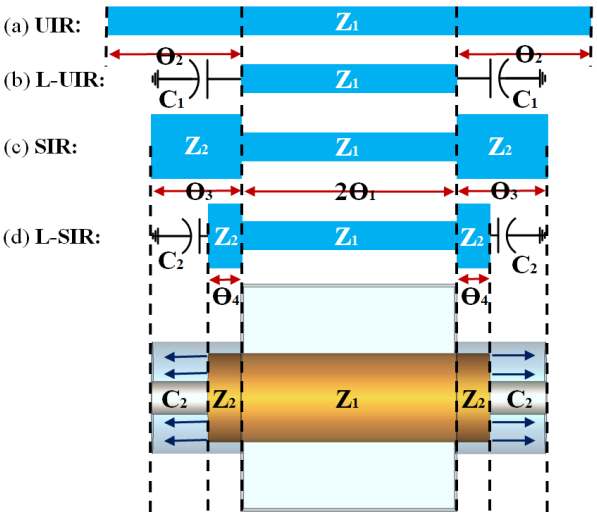

FIGURE 2. Transmission line models of the inset resonator. (a) Uniform Impedance Resonator (UIR), (b) Loaded-Uniform Impedance Resonator (L-UIR), (c) Stepped Impedance Resonator (SIR), (d) Loaded-Stepped Impedance Resonator (L-SIR).

- The longitudinal coupling configuration of the proposed resonator is presented in detail. The capability of obtaining quasi-elliptic responses with flexibly-controllable TZs is explained, and different examples are provided. The implementation feasibility is explored, and a prototype is manufactured and reported.

II. INSET RESONATOR DESIGN AND ANALYSIS

A. INSET RESONATOR STRUCTURE

Fig. 1 depicts a 3D view of the proposed inset resonator configuration. It is comprised of a coaxial resonator inserted partially inside modified portions (sidewall caps) of a metallic housing with the aid of support elements. The resonator can be either metallic for lower cost and excellent spurious performance, or dielectric, offering higher Q and more compactness. This research work deals mainly with metallic resonators as they are more common in applications and also simpler in modeling. The support component is preferably of a low-loss dielectric material with decent strength and acceptable coefficient of thermal expansion (CTE)

(e.g., Teflon, Rexolite). The resonator is centered at the middle of the structure with equal insertion inside both (symmetrical) sidewall caps. This position is for the lowest operational frequency, and it increases with either up or down displacement of the resonator, simultaneously. As shown in Fig. 1, the operating mode is the fundamental transverse-magnetic (TM) mode where the dominant magnetic field resonates in the middle of the resonator assembly, and the electrical field propagates at the top and bottom ends of the resonator where its minima approaches zero at the middle. Hence, despite that any type of resonators can be used in the proposed inset configuration, the TM-mode resonators are particularly the most suitable ones (resonator length > resonator diameter [23]). It can be seen that the inset resonator has similar field patterns to the conventional $\lambda/2$ resonators [1], [2]. However, the inset configuration can advantageously provide substantial size miniaturization and enhanced spurious responses due to the dual capacitive loading effects at both ends of the coaxial resonator caused by the modified sidewall caps.

In comparison with the TEM combline resonators, the inset resonators can feature more compactness with comparable electrical performance. In combline resonators, the magnetic field resonates mainly at the bottom of the cavity while the electrical field is maximum at the vicinity (capacitive gap) between the combline post and the top side of the cavity. Normally, to make the combline structure more compact, the capacitive gap is reduced to increase the capacitive loading and push the resonant frequency lower. Unfortunately, this also leads to a noticeable deterioration in the quality factor due to the high intensity of the E-field in smaller areas which increases the related surface currents and losses. Furthermore, the use of tuning screws will be more critical causing additional ohmic losses and seriously affecting the power handling capabilities of the combline structure. On the contrary in the inset resonator, since the majority of the field is in the middle of the cavity, a relatively low current density is present along the walls of the housing resulting in a higher Q factor. Besides, the sidewall caps are properly designed to contain the lowest field densities. Accordingly, small capacitive gaps (i.e., 0.5 mm) between the caps and the inset resonator can be used, attributing more miniaturization with less sacrifice of quality factor. Here, it should be noted that in the inset resonator, similar to the other configurations, the designer should be aware that the quality factor is usually traded off for reduced mass, size, and complexity. One of the key novelties of the inset resonator structure is the efficient (intrinsic) tuning through the displacement of the coaxial resonator without the need for any auxiliary tuning elements (e.g., screws). Thus, unlike the combline structures, the quality factor remains very stable, as will be shown in the following section.

B. INSET RESONATOR MODEL

Looking at Fig. 2, it can be shown that the inset resonator configuration can be accurately described as a

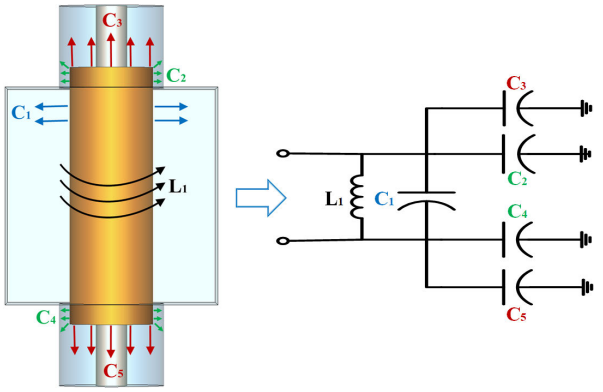

FIGURE 3. Simplified equivalent electrical circuit of the inset resonator.

capacitively-loaded stepped-impedance half-wavelength resonator. To extract the equivalent transmission line model, we begin with an equivalent conventional $\lambda/2$ uniform impedance resonator (UIR) as depicted in Fig. 2(a). The resonator has a uniform impedance Z_1 and a total electrical length $\theta_T = 2\cdot(\theta_1+\theta_2) = \pi$, where $2\cdot\theta_1$ is the height of the metallic housing (H_H) and Z_1 is the characteristic impedance of the coaxial resonator structure excluding the cap sections and can be calculated using [24] and [25]:

$$Z_1 = \frac{60}{\sqrt{\epsilon_r}} \cdot \ln\left(1.079 \cdot \frac{H_W/2}{R_D/2}\right) \tag{1}$$

where ϵ_r is the relative permittivity (equals 1 in vacuum mediums), H_W is the square metallic housing width, and R_D is the coaxial resonator diameter. The next spurious resonance of the UIRs normally appears at $2{\cdot}f_0$ (refer to upcoming equation (7)). Then, the length of the open-end $\lambda/2$ UIR can be shortened and the spurious performance can be enhanced using lumped-element capacitors as depicted in Fig. 2(b). Here, the capacitor-loaded UIR (L-UIR) is more compact than the UIR by a length equal to $2\cdot\theta_2$. The loaded lumped-element capacitors (C_1) can be extracted thru [24]:

$$C_1 = \frac{\tan\theta_2}{Z_1 \cdot \omega_0} \tag{2}$$

where ω_0 is the angular resonant frequency $(=2\cdot\pi\cdot f_0)$, and $\theta_2 = \pi/2 - \theta_1$. Here, C_1 capacitors represent the cap sections including the inserted parts of the coaxial resonator inside them, while $2\cdot\theta_1$ and Z_1 remain unchanged. Alternatively, as the lumped-element capacitors are not convenient for frequencies above 1 GHz, they can be replaced by equivalent transmission line sections representing a stepped impedance resonator (SIR) as can be seen in Fig. 2(c). The SIRs are commonly favorable in a wide range of applications due to their distinct advantage of adjusting the resonator length (hence, frequency), and the spurious resonances with high flexibility and degree of freedom [24], [26]. Similarly, the inset resonator can be modeled as a SIR with two different impedances Z_1 (the metallic housing part) and Z_2 (the caps sections). Whereas Z_1 is known from (1) similar

to the UIR and L-UIR models, Z_2 can be found using [24] and [25]:

$$Z_2 = \frac{60}{\sqrt{\epsilon_r}} \cdot \ln\left(\frac{C_D/2}{R_D/2}\right) \tag{3}$$

where C_D is the diameter of sidewall caps. From this point, the equivalent electrical length of the cap sections θ_3 (and accordingly the overall SIR length $\theta_T = 2 \cdot (\theta_1 + \theta_3)$ can be calculated based on the impedance ratio Z_R (Z_2/Z_1), and θ_1 as follows:

$$\tan\theta_3 = \frac{Z_R}{\tan\theta_1} \tag{4}$$

Also, the SIR total length θ_T can be extracted from [26]:

$$\tan\frac{\theta_T}{2} = \frac{1}{1 - Z_R} \cdot \left(\frac{Z_R}{\tan\theta_1} + \tan\theta_1\right) \tag{5}$$

From this equation, it can be seen clearly the dependence of resonator length on the impedance ratio. When $Z_R = 1$, this is the UIR case where $\theta_T = \pi$. Then, the smaller the impedance ratio than 1 ($Z_2 < Z_1$), the shorter will be the resonator. In addition to the SIR model, the inset resonator can be represented more thoroughly as a loaded SIR where the caps sections and the inserted parts of the coaxial resonator can be regarded as a capacitively-loaded combline posts. Accordingly, the capacitance gap at both ends (C_2) shortens the inset resonator further by a length of $2 \cdot (\theta_3 - \theta_4)$ where θ_3 is known from (4), and θ_4 is the length of the inserted part of the coaxial resonator inside the sidewall caps ($(R_H - H_H)/2$). Similar to (2), C_2 can be expressed as:

$$C_2 = \frac{\tan(\theta_3 - \theta_4)}{Z_2 \cdot \omega_0} \tag{6}$$

Besides the contribution to the inset resonator length adjustment, the impedance ratio also incorporates in controlling the frequency ratio of the first spurious (f_S/f_0) and improving the spurious performance. This relation can be seen clearly in equation (7) below which tells that the frequency ratio increases with the decrease of the impedance ratio [24], [26].

$$\frac{f_S}{f_0} = \frac{\pi}{2 \cdot \tan^{-1}\sqrt{Z_R}} \tag{7}$$

The simplified equivalent electrical circuit of the inset resonator is provided in Fig. 3. The resonant frequency (f_0) can be found based on the cavity inductance (L_1) and the total capacitance (C_T) as follows:

$$f_0 \approx \frac{1}{2 \cdot \pi \cdot \sqrt{L_1 \cdot C_T}} \tag{8}$$

The inductance of the caps sections is relatively small and can be neglected, for simplification. On the other hand, the total capacitance depends on the resonator-housing capacitance (C_1) and the series loading capacitances of the two sidewall caps (C_2, C_3, C_4, C_5):

$$C_T \approx C_1 + ((C_2 + C_3) \parallel (C_4 + C_5)) \tag{9}$$

where C_2 and C_4 represent the resonator-cap capacitance at each side and C_3, C_5 are the loading capacitances of the gap between the resonator and the top and bottom surfaces of the caps, respectively. Then, equation (8) can be re-written as:

$$f_0 \approx \frac{1}{2 \cdot \pi \cdot \sqrt{L_1 \cdot \left(C_1 + \left(\frac{(C_2+C_3)\cdot(C_4+C_5)}{C_2+C_3+C_4+C_5}\right)\right)}} \tag{10}$$

For simplicity, we assume that the two cap sections are symmetrical, and accordingly, C_2=C_4, C_3=C_5. Then, the inductance (L_1), and the different capacitance components can be found as follows [25] and [27]:

$$L_1 \approx \frac{1}{6 \cdot \pi \cdot 10^8} \cdot \sqrt{\frac{\mu_0}{\epsilon_0}} \cdot \ln\left(1.079 \cdot \frac{H_W/2}{R_D/2}\right) \cdot H_H \tag{11}$$

$$C_1 \approx \frac{2 \cdot \pi \cdot H_H}{6 \cdot 10^8 \cdot \sqrt{\frac{\mu_0}{\epsilon_0}} \cdot \ln\left(1.079 \cdot \frac{H_W/2}{R_D/2}\right)} \tag{12}$$

$$C_2, C_4 \approx \frac{2 \cdot \pi \cdot P_H}{6 \cdot 10^8 \cdot \sqrt{\frac{\mu_0}{\epsilon_0}} \cdot \ln\left(\frac{H_W/2}{R_D/2}\right)} \tag{13}$$

$$C_3, C_5 \approx \frac{\epsilon_0 \cdot \pi \cdot (R_D/2)^2}{C_H - P_H} \tag{14}$$

To further validate and confirm the aforementioned conceptualization and models of the proposed inset resonator configuration, a single resonator example is designed, and its different parameters are investigated in detail. The resonator is designed to operate at a resonant frequency of 2.5 GHz. An EM-based model is built and analyzed using the Eigenmode solver in CST microwave studio, while the various transmission line (TL) models and equivalent electrical circuit are calculated using the provided equations and then implemented in ADS circuit simulation environment. The results in Fig. 4 show quite well agreement between the different models in both the resonant frequency at 2.5 GHz and the next spurious resonance at around 8 GHz. The inset resonator is then compared with the conventional combline (reported in [28]) and half-wavelength resonators as summarized in TABLE 1. The coaxial resonator length is 50 mm ($\approx\lambda/2$) in the half-wavelength resonator case, and 25 mm ($\approx\lambda/4$) in the combline and inset configurations. The chosen metal for all components is copper ($\sigma = 5.8\times10^7$ S/m). As is shown, the inset resonator yields a better spurious performance ($3.2 \cdot f_0$), up to more than 60% volume-saving, and a comparable high Q factor with the best Q_u/volume ratio.

TABLE 1. Comparison of the inset resonator with the conventional half-wavelength and combline resonators at 2.5 GHz.

Structure	Half-wavelength	Combline	Inset
f_0 (GHz)	2.5	2.5	**2.5**
f_S (GHz)	5.0	7.4	**8.0**
Q_u	4733	3591	**3536**
Volume (cm^3)	24	12	**8.9**
Q_u/Volume (cm^3)	197.2	299.25	**397.3**

Dimensions (in mm): Half-wavelength: $H_W = 20$, $H_L = 20$, $H_H = 60$, $R_H = 50$, $R_D = 8$. Combline: $H_W = 20$, $H_L = 20$, $H_H = 30$, $R_H = 25$, $R_D = 8$. Inset: $H_W = 20$, $H_L = 20$, $H_H = 21$, $R_H = 25$, $R_D = 8$, $C_H = 4$, $C_D = 9$. The material of all metallic parts is copper.

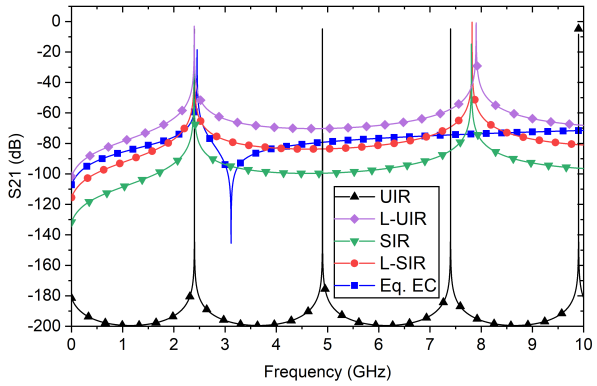

FIGURE 4. Transmission coefficient responses of various inset resonator TL models and equivalent electrical circuit at 2.5 GHz. The corresponding physical dimensions are in TABLE 1. Black line: uniform impedance resonator ($Z_1 = 59.54\ \Omega$, $\theta_1 = 63^o$, $\theta_2 = 58.5^o$). Violet line: loaded-uniform impedance resonator ($C_1 = 1.75$ pF). Green line: stepped impedance resonator ($Z_2 = 7.066\ \Omega$, $\theta_3 = 10.99^o$). Red line: loaded-stepped impedance resonator ($\theta_4 = 6^o$, $C_2 = 0.787$ pF). Blue line: equivalent electrical circuit ($L_1 = 4.153$ nH, $C_1 = 0.59$ pF, C_2, $C_4 = 0.472$ pF, C_3, $C_5 = 0.222$ pF).

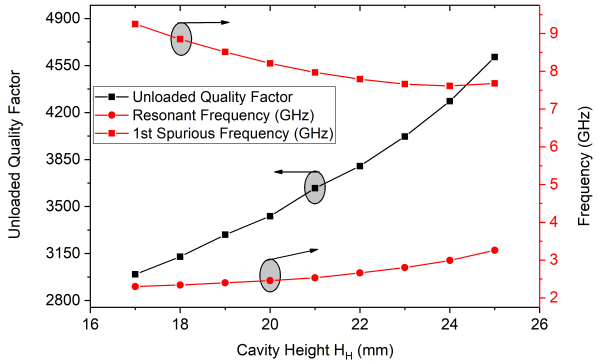

FIGURE 5. Dependence of the fundamental frequency, 1st spurious resonance, and unloaded quality factor on the height of the metallic housing (H_H). The corresponding physical dimensions are in TABLE 1.

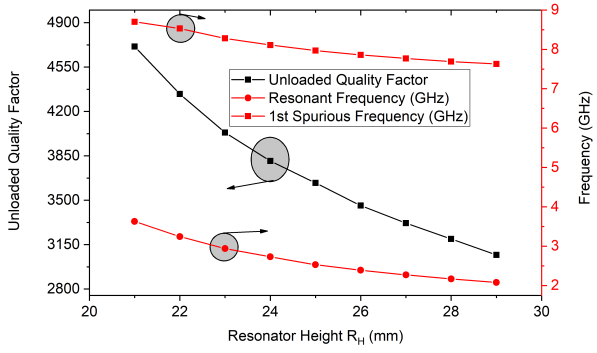

FIGURE 6. Fundamental frequency, 1st spurious resonance, and unloaded quality factor with respect to resonator height (R_H). The corresponding physical dimensions are in TABLE 1.

Next, the different design parameters (the housing, resonator, and sidewall caps) of the presented inset resonator are studied. Fig. 5 and Fig. 6 depict the variation in the resonant frequency, 1st spurious resonance, and unloaded Q factor with respect to

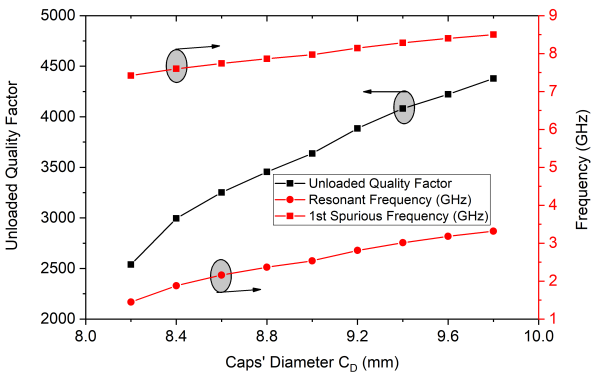

FIGURE 7. Fundamental frequency, 1st spurious resonance, and unloaded quality factor with respect to the caps' diameter (C_D).The corresponding physical dimensions are in TABLE 1.

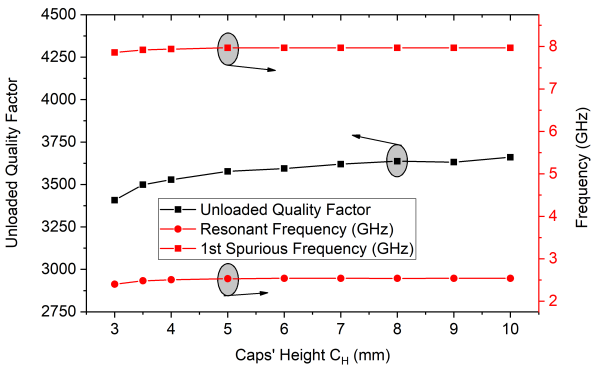

FIGURE 8. Fundamental frequency, 1st spurious resonance, and unloaded quality factor with respect to the cap's height (C_H). The corresponding physical dimensions are in TABLE 1.

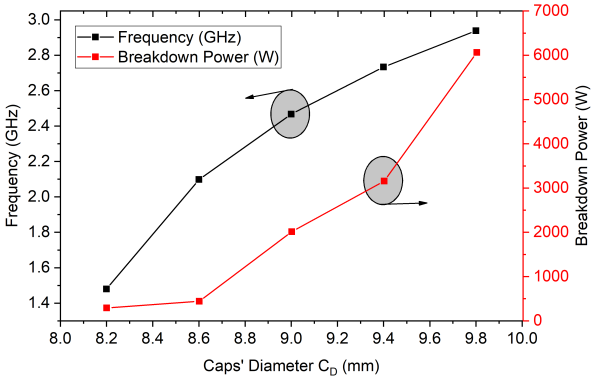

FIGURE 9. Center-frequency and power breakdown level with respect to the cap's diameter (C_D). The corresponding physical dimensions are in TABLE 1.

the housing height (H_H) and resonator length (R_H), respectively. When the H_H is reduced, this means more parts of the resonator will be inserted into the sidewall caps. Consequently, the corresponding capacitance components will increase (C_2, C_3, C_4, C_5) and move the resonant frequency lower based on equation (10). Besides, an improvement in the spurious separation can be noticed. The same happens

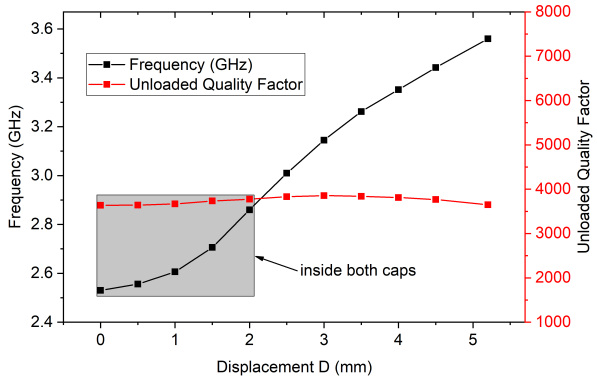

FIGURE 10. Fundamental frequency and unloaded quality factor variation with respect to inset resonator displacement. The corresponding physical dimensions are in TABLE 1 ($C_H = 8$ mm).

when the resonator is elongated as can be seen in Fig. 6. In both cases, this will be accompanied by a variation in the quality factor. The sidewall caps are the most important part of the inset resonators and should be designed properly based on the desired requirements. Fig. 7 describes the impact of the caps' diameter (C_D) on the frequency and the Q factor. The smaller the gap between the cap and the resonator, the smaller the corresponding impedance Z_2 (refer to equation (3)) will be. Consequently, based on equations (5) and (7), the resonant frequency will be shifted downwards, and the spurious performance will improve. Fig. 8 relates the frequency and quality factor to the change in the caps' height (C_H). Since the contained fields inside the caps are relatively small, we can see that the resonant frequency and the Q factor remain almost constant and stable. This feature is particularly useful for the design of tunable inset structures [21] where the caps are designed based on the required room for the movable inset resonators to obtain the desired tuning. Apart from that, the resonant frequency can still be decreased by further reducing the capacitive gap between the resonator and the caps, and increasing the corresponding capacitances C_3, C_5. Since relatively small gaps are needed between the resonator and the caps (i.e. 0.5 mm) for higher miniaturization, some worries might be raised regarding the power handling capabilities of the proposed inset resonator configuration. Therefore, we have investigated this using the Sparks3D tool in CST with different gaps sizes between the caps and the resonator. It is evident in Fig. 9 that the resonator can handle power levels of more than 2000 W while the gap size is of only 0.5 mm. It can be further improved up to 6000 W by increasing the gap size. Additionally, it was shown in [29] that lamination with a dielectric material (e.g., Teflon) can further enhance the power handling capabilities.

One of the key advantages of the inset resonator configuration is the ability to tune the resonant frequency through the displacement of the coaxial resonator without the need for any additional tuning elements. As mentioned earlier this so-called "*self-tuning*" simplifies the tuning process and is able maintain a stable Q factor. Fig. 10 shows the tuning capabilities of the presented inset resonator. Here, we extended the height of the caps by 4 mm (C_H=8 mm) to offer more room for the resonator displacement and provide higher tunability. When the resonator is displaced from the center, the resonant frequency will increase due to the change in the loading capacitances at both ends (refer to Fig. 3, eqs. (9) and (10)). For post-tuning of microwave filters, we normally require fine-tuning elements for a small frequency range. Therefore, the designer can move the resonator slightly to adjust the resonant frequency (e.g., within the shaded gray box at Fig. 10, where the resonator is inside both caps). Of course, further tuning can be obtained as can be seen, which is useful for tunable filter applications as detailed in [22]. The most interesting feature of this tuning mechanism is that the Q factor remains stable with minimum variation throughout the tuning window.

III. QUASI-ELLIPTIC INSET FILTERS

This section presents quasi-elliptic filter designs in planar and longitudinal coupling configurations based on the proposed inset-type resonator. In general, the filter design procedure begins with the desired electrical and physical specifications including the quality factor, spurious-free band, stopband rejection level, maximum RF power, and volume. Then, the inset resonator cavities are designed carefully to meet these requirements as detailed in the previous section II, and the filter unit is built with proper iris and input-output structures.

A. INSET FILTERS IN PLANAR CONFIGURATION

In this part, a compact fourth-order coaxial inset filter is presented in a planar coupling configuration. The filter is built in a folded topology to realize a cross-coupling and create transmission zeros. Fig. 11 shows a perspective view of the quasi-elliptic four-pole filter designed to operate at 2.8 GHz with a bandwidth of 75 MHz, Q_u of 3100 (with copper), and two symmetrical transmission zeros. It is worth to note that this filter is also designed for tunable applications, but, will not discuss it here as we are only interested in its fixed version (for tunable configurations, please refer to ref. [22]). Based on the specifications, the corresponding coupling matrix is extracted following the standard synthesis procedure [30]:

$$\begin{bmatrix} & S & 1 & 2 & 3 & 4 & L \\ S & 0 & 1.04 & 0 & 0 & 0 & -0.0003 \\ 1 & 1.04 & 0 & 0.91 & 0 & 0 & 0 \\ 2 & 0 & 0.91 & 0 & 0.70 & 0 & 0 \\ 3 & 0 & 0 & 0.70 & 0 & 0.91 & 0 \\ 4 & 0 & 0 & 0 & 0.91 & 0 & 1.04 \\ L & -0.0003 & 0 & 0 & 0 & 1.04 & 0 \end{bmatrix} \quad (15)$$

Next, the required physical input-output (IO) and inter-resonator couplings are realized. As shown in Fig. 11, the IO couplings are obtained using inductive coupling posts fed through Sub-Miniature version A (SMA) connectors. Similarly, the required physical inter-resonator couplings are realized by properly adjusting the dimensions of the iris sections.

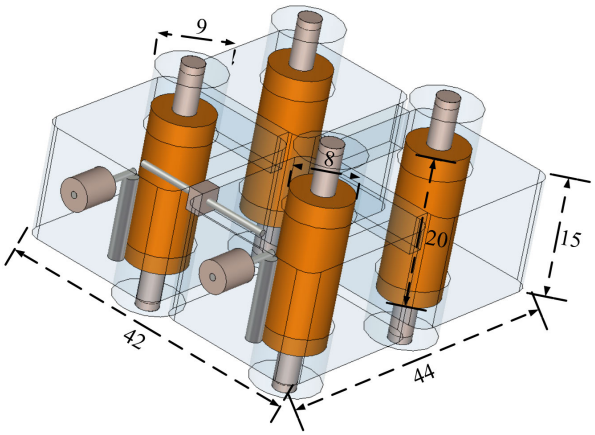

FIGURE 11. 3D structure of the proposed folded 4th-order coaxial inset filter. All dimensions are in mm unit.

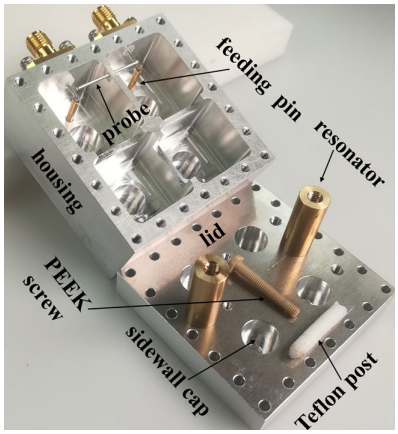

FIGURE 12. The fabricated folded four-pole inset filter (disassembled).

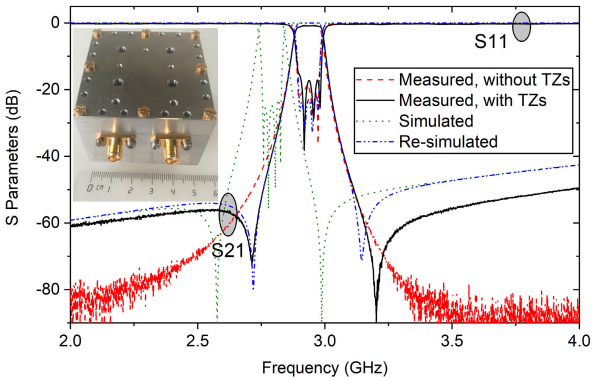

FIGURE 13. Simulated and measured results of the folded 4th-order inset filter.

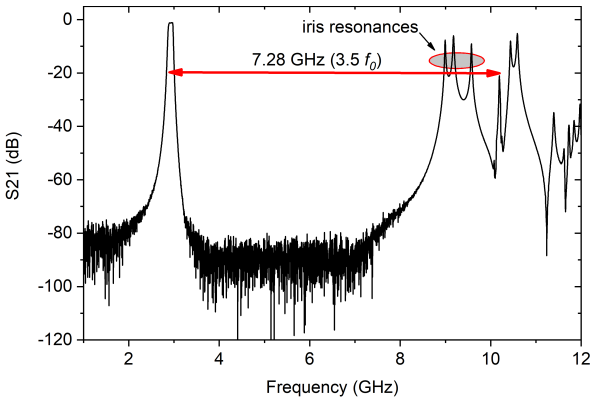

FIGURE 14. Wideband response of the four-pole inset filter.

A capacitive coupling probe is used to realize a source-load coupling path introducing two symmetrical transmission zeros as exhibited in Fig. 13. A prototype is then manufactured and assembled as depicted in Fig. 12 and Fig. 13, respectively. The metallic housing is made of aluminum, while the coaxial resonators are milled out of brass metal. The resonators are positioned using Polyetheretherketone (PEEK) screws at one end (which are more durable than the Teflon screws) with the aid of Teflon posts at the other end. The overall volume of the filter prototype is $54\times52\times35$ mm^3.

The measured results of the proposed folded filter are presented in Fig. 13 with and without the capacitive coupling probe (with and without TZs). The filter is centered at 2.93 GHz with a mid-band insertion loss better than 0.73 dB, a return loss higher than 18 dB, and extracted quality factor of 1000. It is worth mentioning that no tuners are employed. A 4.6% increase is noticed from the simulated operating frequency (2.8 GHz). This is mainly due to manufacturing tolerances, particularly in the caps' sections which are the most sensitive parts. Hence, the simulations were optimized to resemble the measurements through decreasing the gap between the coaxial resonators and the caps by 0.08 mm. To compensate for this increase in frequency, tuning screws can be introduced, however, this is not a favorable option in many applications as discussed earlier. Alternatively, it is more convenient for designers to consider the manufacturing tolerances in advance to get an excellent agreement. For example, a second version of this filter can be designed at a 4.6% lower frequency ($\approx$ 2.67 GHz). Then, if a further up-tuning is required, the resonators can be displaced accordingly. In this manner, the need for additional tuning screws (to decrease the resonant frequency) can be eliminated. Another possible option since that the coaxial resonators are separated components, they can be simply replaced by longer ones (could save cost and time). The wideband response of the implemented filter is demonstrated in Fig. 14. The next spurious frequency is at $3.5{\cdot}f_0$, while the iris resonances can be noticed at $\approx 3{\cdot}f_0$, which can be redesigned to suppress their unwanted resonances.

B. INSET FILTERS IN LONGITUDINAL CONFIGURATION

As we earlier discussed, there is a fundamental need for inline coaxial filter configurations that are able to introduce TZs with flexible positioning. With regard to this, another possible setup of the inset resonator filters is the inline longitudinal configuration. Besides to the more compact structures, compared with the aforementioned planar topology, the

longitudinal inset configuration has the capability of obtaining quasi-elliptic responses in inline arrangements. For instance, Fig. 15 illustrates a 3rd-order inset filter that operates at 3.08 GHz with a bandwidth of 56 MHz and unloaded quality factor about 2720 (with copper). The couplings between the adjacent resonators (inter-resonator couplings) are magnetic-based (inductive) couplings. In addition, there is a transmission zero that can be seen relatively far away from the passband at 2.55 GHz. This TZ is created through a relatively weak electrically dominant (capacitive) coupling path between the nonadjacent resonators (1 and 3). This TZ can be moved closer to the passband by increasing the electrical coupling strength between the resonators. Referring to Fig. 1, we know that the E-field is mainly focused at the ends of the inset resonators. Consequently, the E-field coupling strength can be increased effectively by: 1) making central openings in the irises, so, the adjacent resonators' ends face each other directly, and then, 2) moving the resonators closer. Simultaneously, the irises and the resonant frequency of each cavity must be re-optimised to provide the same operating frequency and bandwidth. Fig. 16(a) presents a design example which has similar passband specifications to the above filter (i.e., f_0=3.08 GHz, BW=56 MHz), but, the TZ is moved and positioned very close to the passband at 2.98 GHz. Additionally, the TZ can be flexibly shifted to the upper side by simply changing the sign of any inter-resonator coupling pair (m_{12} or m_{23}). This is realized by rotating the respective coupling iris by 180^o angle as can be seen in the filter-2 example in Fig. 16(b). This advantage of introducing flexibly controllable TZs distinguishes the proposed inset configuration from similar longitudinally-coupled loaded-waveguide filters available in the literature [12], [14], [31], [32], [33]. While the inline coaxial filter in [12] and the electrically-coupled TM-mode dielectric filters in [31], [32], and [33] cannot introduce TZs, the TZ controllability was not demonstrated in the additively-manufactured combline filter in [14].

Regarding the realization of the longitudinal inset filters, a common dielectric support element can be used to fix all resonators in their required positions, simultaneously. Alternatively, side support elements can be used to fix each resonator independently as it shown in Fig. 15(a). The support element is preferably to be positioned at the middle of the resonator where the E-field is minimum (almost zero). Accordingly, the side support will have a minimum impact on the resonant frequency and the quality factor, and can be either dielectric or metallic. This could allow for monolithic additive manufacturing which helps in reducing the assembly-related errors and losses. This would be even more beneficial as frequency tuning is more challenging in longitudinal configurations than in the planar ones, because the resonators cannot be displaced independently.

To experiment the feasibility of implementing such structures using the conventional CNC machining, a 3rd-order filter is designed and manufactured. The filter shown in Fig. 17 is designed to operate at 2.69 GHz with a bandwidth

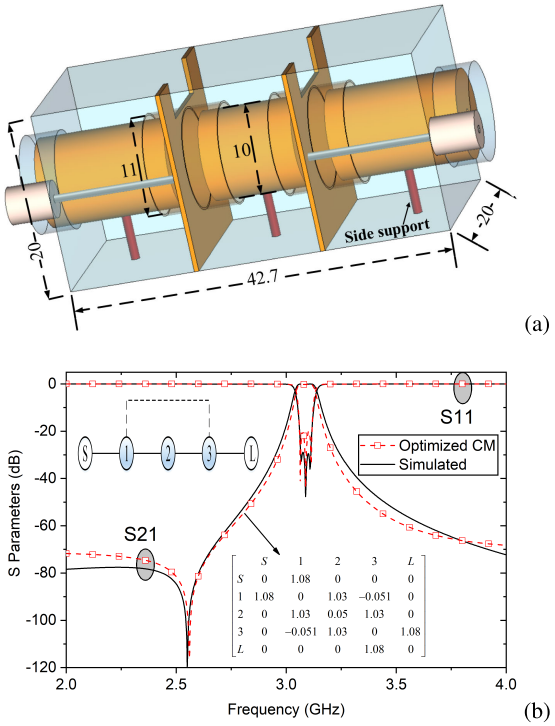

FIGURE 15. Third-order inset filter in a longitudinal configuration. (a) 3D structure (in mm unit) and (b) simulated (solid black line) and optimized coupling matrix (dashed red line).

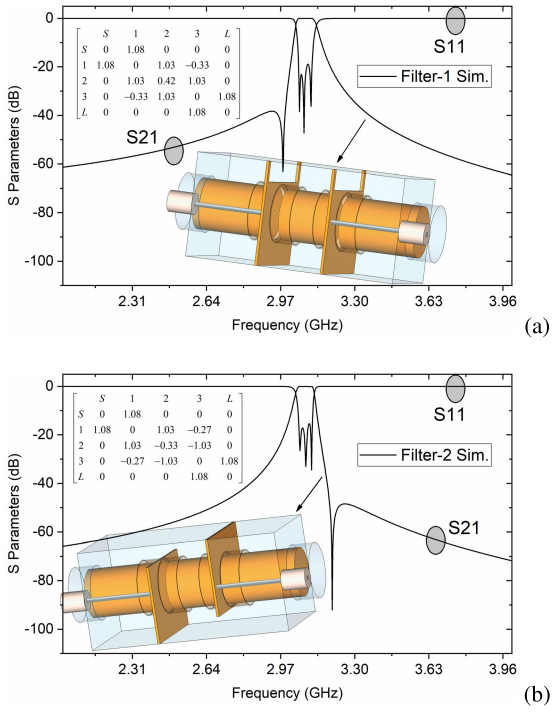

FIGURE 16. Longitudinal inset filters with similar frequency and bandwidth of the previous example in Fig. 15. (a) Filter-1: Close transmission zero at the lower stopband. (b) Filter-2: Close transmission zero at the upper stopband.

of 81 MHz and a lower transmission zero at 2.48 GHz with a 50 dB rejection level. The simulated quality factor is around 2820 when using copper metal ($\sigma = 5.8\times10^7$ S/m) and

TABLE 2. Comparison of the proposed tunable inset filters with similar state-of-the-art designs.

Ref.	Configuration	f_0 (GHz)	Order	BW (MHz)	TZs	IL (dB)	Q-factor	f_S (GHz)	Size (λ_g^3)
[7]	folded SIR combline	2.58	4	98	3	0.25	2900	NA	0.012
[11]	folded re-entrant combline	1.54	6	49	2	0.86	NA	$2.34f_0$	0.105
[14]	inline longitudinal combline	3.51	3	235	1	≥ 0.09	2461	$3.13f_0$	NA
[15]	folded combline	2.0175	4	15	2	0.65	NA	NA	0.074
[17]	inline orthogonal combline	1.54	6	48.8	2	NA	4400	$2.7f_0$	0.039
[18]	inline orthogonal combline	2.14	6	60	2	NA	NA	$2.2f_0$	0.043
This work-1	**folded inset**	**2.93**	**4**	**82**	**2**	**0.73**	**1000**	$\mathbf{3.5}f_0$	**0.029**
This work-2	**inline longitudinal inset**	**2.53**	**3**	**120**	**1**	**0.45**	**800**	$\mathbf{3}f_0$	**0.016**

Ref.= reference, f_0= resonant frequency, IL= insertion loss, f_S= spurious frequency, λ_g= guided wavelength at the operating frequency.

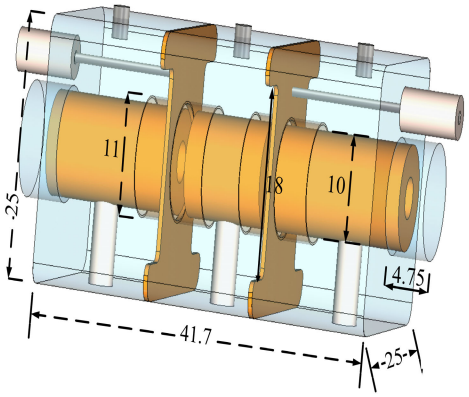

FIGURE 17. 3D structure of the proposed longitudinal three-pole coaxial inset filter at 2.69 GHz. All dimensions are in mm unit.

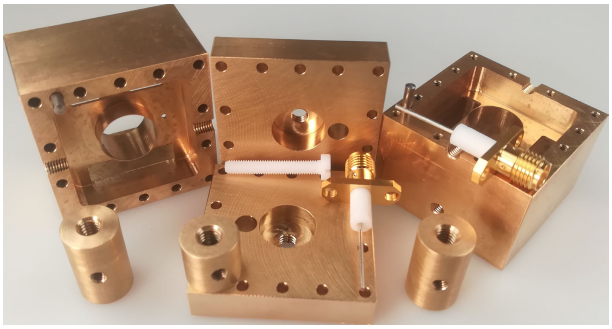

FIGURE 18. The fabricated longitudinal inset filter. (a) Disassembled parts. (b) Measured vs. simulated results.

1470 with brass ($\sigma = 1.59\times10^7$ S/m). The resonators are fixed in their positions using M3 Teflon screws from one side, while metallic M3 screws are introduced at the other side for tuning purposes. Unlike the filter example in Fig. 15(a) with single-sided irises, slots are made here at two sides to increase the inter-resonator coupling strength for a wider bandwidth. The filter prototype parts were manufactured using brass alloy and then assembled as exhibited in Fig. 18. The filter prototype has a compact volume of $55.7\times33\times33$ mm^3. The measured results in Fig. 18(b) show that the filter is centered at 2.53 GHz with a BW of 120 MHz, a midband insertion loss better than 0.45 dB, and a return loss higher than 12.5 dB. The estimated unloaded quality factor is around 800 (54% of simulated Q). Also, a 60 dB lower stopband transmission zero is introduced at $\approx$ 2.11 GHz. A 160 MHz frequency decrease from simulated results is noticed due to the manufacturing and assembly tolerances, mainly at the caps sections (re-simulations estimate caps' radii smaller by 0.09 mm). As result, the electrical coupling decreases (hence, the TZ is pushed further), and the inter-resonator (magnetic) couplings increase (thus, the BW becomes wider). The response can be conveniently recovered similar to the earlier prototype in the above sub-section. Besides, silver-plated M3 screws were added to provide additional tuning. The next spurious resonance frequency is noticed at 7.43 GHz ($\approx3\cdot f_0$); it can be suppressed further up to 8.89 GHz ($\approx3.5\cdot f_0$) with proper design procedure.

A comparison between the proposed inset filters and similar quasi-elliptic coaxial BPFs is summarized in TABLE 2. As apparent, the inset-based designs provide the merits of volume miniaturization and enhanced spurious performance,

in addition to the capability of obtaining flexibly controllable quasi-elliptic responses. The first planar configuration in section III-A follows the common folded topology to realize a cross-coupling and create TZs, similar to [7], [11], and [15]. Also, as the inline structure is favourable in many applications, [17] and [18] used orthogonal combline resonators to introduce TZs. Nevertheless, these designs are complex in manufacturing and have a degraded spurious performance. Whereas in [14], the compact vertical combline structure allowed the cross-coupling between the non-adjacent resonators to happen and generate a single TZ. However, it has a major limitation in controlling the TZ position. Contrary, in the presented longitudinal inline configuration of the inset filters, transmission zeros can be adjusted flexibly and effectively.

IV. CONCLUSION

The design and analysis of a novel inset resonator configuration are presented in this paper for coaxial filter applications. The inset configuration has several desirable characteristics including the miniaturized size, high-quality factor, ability to handle relatively high levels of power, and very good spurious performance ($>3{\cdot}f_0$). Furthermore, the inset resonator structure has a distinct feature of *self-tuning* without the need for any auxiliary tuning elements, attributing stable high-Q performance with minimum variation. Different coaxial inset filters are reported using planar and longitudinal coupling configurations with the capability of obtaining quasi-elliptic responses in inline structures and flexible control of transmission zeros. All these competitive merits promote the new inset configuration in a wide range of coaxial filter applications (e.g., cellular base stations and tunable filters).

REFERENCES

[1] G. Basavarajappa and R. R. Mansour, "Design methodology of a high-Q tunable coaxial filter and diplexer," *IEEE Trans. Microw. Theory Techn.*, vol. 67, no. 12, pp. 5005–5015, Dec. 2019, doi: 10.1109/TMTT.2019.2937770.

[2] M. Yu, D. Smith, and M. Ismail, "Half-wave dielectric rod resonator filter," in *IEEE MTT-S Int. Microw. Symp. Dig.*, Jun. 2004, pp. 1601–1604, doi: 10.1109/MWSYM.2004.1336060.

[3] M. Makimoto and S. Yamashita, "Compact bandpass filters using stepped impedance resonators," *Proc. IEEE*, vol. 67, no. 1, pp. 16–19, Jan. 1979, doi: 10.1109/PROC.1979.11196.

[4] H. Wang and Q.-X. Chu, "An inline coaxial quasi-elliptic filter with controllable mixed electric and magnetic coupling," *IEEE Trans. Microw. Theory Techn.*, vol. 57, no. 3, pp. 667–673, Mar. 2009, doi: 10.1109/TMTT.2009.2013290.

[5] H.-H. Chen, R.-C. Hsieh, Y.-T. Shih, Y.-H. Chou, and M.-H. Chen, "Coaxial combline filters using the stepped-impedance resonators," in *Proc. Asia–Pacific Microw. Conf.*, 2010, pp. 1724–1727.

[6] F. Gentili, L. Pelliccia, R. Sorrentino, and G. Bianchi, "High Q-factor compact filters with wide-band spurious rejection," in *Proc. 42nd Eur. Microw. Conf.*, Oct. 2012, pp. 160–163, doi: 10.23919/EuMC.2012.6459271.

[7] X. Wang, G. Jang, B. Lee, and N. Park, "Compact quad-mode bandpass filter using modified coaxial cavity resonator with improved Q-factor," *IEEE Trans. Microw. Theory Techn.*, vol. 63, no. 3, pp. 965–975, Mar. 2015, doi: 10.1109/TMTT.2015.2389231.

[8] C. Tomassoni, G. Venanzoni, M. Dionigi, and R. Sorrentino, "Compact quasi-elliptic filters with mushroom-shaped resonators manufactured with 3-D printer," *IEEE Trans. Microw. Theory Techn.*, vol. 66, no. 8, pp. 3579–3588, Aug. 2018, doi: 10.1109/TMTT.2018.2849067.

[9] E. Musonda and I. C. Hunter, "Microwave bandpass filters using re-entrant resonators," *IEEE Trans. Microw. Theory Techn.*, vol. 63, no. 3, pp. 954–964, Mar. 2015, doi: 10.1109/TMTT.2015.2389216.

[10] E. Doumanis, S. Bulja, and D. Kozlov, "Compact coaxial filters for BTS applications," *IEEE Microw. Wireless Compon. Lett.*, vol. 63, no. 3, pp. 954–964, Mar. 2015, doi: 10.1109/LMWC.2017.2757446.

[11] J. Benedicto, E. Rius, J.-F. Favennec, D. Pacaud, L. Carpentier, and J. Puech, "A compact L-band bandpass filter based on SIR coaxial resonators with high multipactor threshold," *Int. J. Microw. Wireless Technol.*, vol. 14, no. 3, pp. 270–281, Apr. 2022, doi: 10.1017/s1759078720001786.

[12] M. Salek, X. Shang, and M. J. Lancaster, "Compact S-band coaxial cavity resonator filter fabricated by 3-D printing," *IEEE Microw. Wireless Compon. Lett.*, vol. 29, no. 6, pp. 382–384, Jun. 2019, doi: 10.1109/LMWC.2019.2913155.

[13] E. Lopez-Oliver, C. Tomassoni, L. Silvestri, M. Bozzi, L. Perregrini, S. Marconi, G. Alaimo, and F. Auricchio, "3-D-printed compact bandpass filters based on conical posts," *IEEE Trans. Microw. Theory Techn.*, vol. 69, no. 1, pp. 616–628, Jan. 2021, doi: 10.1109/TMTT.2020.3035168.

[14] K. Zhao and D. Psychogiou, "A monolithic vertical integration concept for compact coaxial-resonator-based bandpass filters using additive manufacturing," *IEEE Microw. Wireless Compon. Lett.*, vol. 31, no. 6, pp. 689–692, Jun. 2021, doi: 10.1109/LMWC.2021.3062825.

[15] M. Höft, S. Burger, T. Magath, and O. Bartz, "Compact combline filter with improved cross coupling assembly and temperature compensation," in *Proc. Asia–Pacific Microw. Conf.*, Dec. 2006, pp. 781–784, doi: 10.1109/APMC.2006.4429531.

[16] M. Höft, "Tunable capacitive coupling for cavity resonator filters," in *Proc. German Microw. Conf.*, Mar. 2009, pp. 1–4.

[17] Y. Wang and M. Yu, "True inline cross-coupled coaxial cavity filters," *IEEE Trans. Microw. Theory Techn.*, vol. 57, no. 12, pp. 2958–2965, Dec. 2009, doi: 10.1109/TMTT.2009.2034221.

[18] M. Höft and F. Yousif, "Orthogonal coaxial cavity filters with distributed cross-coupling," *IEEE Microw. Wireless Compon. Lett.*, vol. 21, no. 10, pp. 519–521, Oct. 2011, doi: 10.1109/LMWC.2011.2165533.

[19] G. Macchiarella, S. Bastioli, and R. Snyder, "Design of in-line filters with transmission zeros using strongly-coupled resonators pairs," *IEEE Trans. Microw. Theory Tech.*, vol. 66, no. 8, pp. 3836–3846, Aug. 2018, doi: 10.1109/TMTT.2018.2840981.

[20] S. Bastioli, R. V. Snyder, and G. Macchiarella, "Design of in-line filters with strongly coupled resonator triplet," *IEEE Trans. Microw. Theory Techn.*, vol. 66, no. 12, pp. 5585–5592, Dec. 2018, doi: 10.1109/TMTT.2018.2867004.

[21] A. Widaa, C. Bartlett, and M. Höft, "Inset resonators and their applications in fixed/reconfigurable microwave filters," in *IEEE MTT-S Int. Microw. Symp. Dig.*, Jun. 2022, pp. 172–175, doi: 10.1109/IMS37962.2022.9865311.

[22] A. Widaa, C. Bartlett, and M. Höft, "Tunable coaxial bandpass filters based on inset resonators," *IEEE Trans. Microw. Theory Techn.*, vol. 71, no. 1, pp. 285–295, Jan. 2023, doi: 10.1109/TMTT.2022.3222321.

[23] C. Wang and K. A. Zaki, "Dielectric resonators and filters," *IEEE Microw. Mag.*, vol. 8, no. 5, pp. 115–127, Oct. 2007, doi: 10.1109/MMM.2007.903648.

[24] M. Makimoto and S. Yamashita, *Microwave Resonators and Filters for Wireless Communication: Theory, Design and Application*, vol. 4. New York, NY, USA: Springer, 1994, pp. 19–101.

[25] A. Anand and X. Liu, "Reconfigurable planar capacitive coupling in substrate-integrated coaxial-cavity filters," *IEEE Trans. Microw. Theory Techn.*, vol. 64, no. 8, pp. 2548–2560, Aug. 2016, doi: 10.1109/TMTT.2016.2580140.

[26] M. Makimoto and S. Yamashita, "Bandpass filters using parallel coupled stripline stepped impedance resonators," *IEEE Trans. Microw. Theory Techn.*, vol. MTT-28, no. 12, pp. 1413–1417, Dec. 1980, doi: 10.1109/TMTT.1980.1130258.

[27] Z.-A. Yang, D. Psychogiou, and D. Peroulis, "Design and optimization of tunable silicon-integrated evanescent-mode bandpass filters," *IEEE Trans. Microw. Theory Techn.*, vol. 66, no. 4, pp. 1790–1803, Apr. 2018, doi: 10.1109/TMTT.2018.2799575.

[28] D. Sh-Asanjan and R. R. Mansour, "A novel coaxial resonator for high power applications," in *Proc. 44th Eur. Microw. Conf.*, Oct. 2014, pp. 295–298, doi: 10.1109/EuMC.2014.6986428.

[29] C. Rong, Y. Xu, and Y. Zhang, "Dielectric-loaded miniaturized cavity bandpass filter with improved power capacity," *Electronics*, vol. 11, no. 9, p. 1441, Apr. 2022, doi: 10.3390/electronics11091441.

[30] R. J. Cameron, C. M. Kudsia, and R. R. Mansour, *Microwave Filters for Communication Systems: Fundamentals, Design, and Applications*. Hoboken, NJ, USA: Wiley, 2018.
[31] Y. Kobayashi, K. Kojima, and S. Yoshida, "Bandpass filters using electrically-coupled TM_{010} dielectric rod resonators," *Electron. Commun. Jpn.*, vol. 66, no. 3, pp. 33–42, 1983, doi: 10.1002/ecja.4400660306.
[32] Y. Marchives, N. Delhote, S. Verdeyme, and P. M. Iglesias, "Wideband dielectric filter at C-band manufactured by stereolithography," in *Proc. 44th Eur. Microw. Conf.*, Oct. 2014, pp. 187–190, doi: 10.1109/EuMC.2014.6986401.
[33] A. Widaa, F. Cacciamani, L. Pelliccia, C. Tomassoni, V. T. Di Crestvolant, and M. Hoft, "Compact ultra-wideband bandpass filter using additively manufactured TM-mode dielectric resonators," in *Proc. 52nd Eur. Microw. Conf. (EuMC)*, Sep. 2022, pp. 115–118, doi: 10.23919/EuMC54642.2022.9924504.

ABDULRAHMAN WIDAA (Graduate Student Member, IEEE) was born in Wad Medani, Gezira, Sudan, in 1991. He received the B.Sc. degree (Hons.) in telecommunication engineering from the University of Gezira, Wad Madani, in 2014, and the M.Eng. degree in information and communication engineering from the University of Electronic Science and Technology of China, Chengdu, China, in 2018. He is currently pursuing the Dr.-Ing. degree in electrical and information engineering with Kiel University, Kiel, Germany.

From 2014 to 2016, he was a Teaching Assistant with the Electronics Engineering Department, University of Gezira. From 2016 to 2018, he was a Research Assistant with the University of Electronic Science and Technology of China, where he was involved in the design of tunable filters for RF/microwave applications. From 2018 to 2019, he was a Lecturer with the Electronics Engineering Department, University of Gezira. He was a Visiting Researcher with Technische Universität Darmstadt, Darmstadt, Germany, from February 2020 to March 2020; the University of Perugia, Perugia, Italy; RF Microtech S.r.l, Perugia, from May 2021 to July 2021; and the Universitat Politècnica de València, Valencia, Spain, from April 2022 to May 2022. Since 2019, he has been a Researcher with the Chair of Microwave Engineering, Kiel University, under the European Union's Project of Advanced Technologies for Future European Satellite Applications (TESLA). His research interests include design of miniaturized/tunable filters and components for microwave and satellite communications, sensors, and embedded systems.

Mr. Widaa was a recipient of many national and international awards, scholarships, and grants, including the Chinese University Master Scholarship Program in 2016 and the European Microwave Week Student Grant in 2020 and 2021.

CHAD BARTLETT (Graduate Student Member, IEEE) was born in Nelson, BC, Canada, in 1987. He received the B.Eng. and M.A.Sc. degrees in electrical engineering from the University of Victoria, Victoria, BC, in 2017 and 2019, respectively. He is currently pursuing the Dr.-Ing. degree with the Chair of Microwave Engineering, Department of Electrical and Information Engineering, Kiel University, Kiel, Germany. His primary research interests include microwave and millimeter-wave passive components, filters, and antenna networks for the next generation of satellite and communication systems, and developing methods for overcoming challenges in micro-scale designs. He is a member of the European Union's Horizon 2020 Research and Innovation Program for Early-Stage Researchers.

MICHAEL HÖFT (Senior Member, IEEE) was born in Lübeck, Germany, in 1972. He received the Dipl.-Ing. degree in electrical engineering and the Dr.-Ing. degree from the Hamburg University of Technology, Hamburg, Germany, in 1997 and 2002, respectively. From 2002 to 2013, he joined the Communications Laboratory, European Technology Center, Panasonic Industrial Devices Europe GmbH, Lüneburg. He was a Research Engineer and then a Team Leader, where he was engaged in research and development of microwave circuitry and components, particularly filters for cellular radio communications. From 2010 to 2013, he was a Group Leader of research and development of sensor and network devices. Since October 2013, he has been a Full Professor with the Faculty of Engineering, Kiel University, Kiel, Germany, where he is currently the Head of the Chair of Microwave Engineering, Department of Electrical and Information Engineering. His research interests include active and passive microwave components, submillimeter-wave quasioptical techniques and circuitry, microwave and field measurement techniques, microwave filters, microwave sensors, and magnetic field sensors. He is a member of the European Microwave Association (EuMA), the Association of German Engineers (VDI), and the German Institute of Electrical Engineers (VDE).